



# EVALUATION OF THE USE OF CONSTRAINTS IN STEP-BY-STEP ALGORITHMS FOR THE SOLUTION OF A 2D INVERSE HEAT TRANSFER PROBLEM

Rodrigo Vidonsky Pinto<sup>a</sup>, Flávio Augusto Sanzovo Fiorelli<sup>b,\*</sup>

<sup>a</sup> University Centre of United Metropolitan Faculties, Dept. of Mechanical Engineering - São Paulo, SP, 04505-002, Brazil

<sup>b</sup> Escola Politécnica, University of Sao Paulo - Dept. of Mechanical Engineering, Sao Paulo, SP, 05508-030, Brazil

## ABSTRACT

The present paper provides a discussion about the use of constraints in step-by-step optimization algorithms used for the solution of a two-dimensional inverse heat transfer problem containing a modeling error. It is observed that the unrestricted algorithms provided better estimates to the power map and the introduction of constraints is harmful to the solution of the inverse heat transfer problem, reducing the area in which this solution approaches the actual heat sources distribution, due to the solution of the unrestricted problem adopting negative values in restricted areas, which compensate the high sensitivity of this problem and consequently provide improved solutions.

**Keywords:** Inverse Heat Transfer. Constraints. Optimization.

## 1. INTRODUCTION

The recent development of advanced techniques for the local cooling of the hotspots formed in the operation of a computer microprocessor, such as the use of high-velocity impingement jets produced by piezoelectric fans (Velardo *et al.*, 2021) and microchannel cooling systems (Gulia and Sur, 2022), resulted in a direct concern with the solution of two-dimensional inverse heat transfer problems such that the correct location and intensity of these hotspots could be provided to the application of these techniques.

The direct two-dimensional steady heat transfer problem applied to these electronic devices is defined by the normalized steady-state heat diffusion equation:

$$\nabla \cdot [k \cdot \nabla \theta] - h \cdot \theta + S = 0 \quad (1)$$

$$\theta = T - T_{\infty} \quad (2)$$

Such that the heat sources distribution  $S$  is previously known and defined as a boundary condition, as well as the geometrical boundaries of the domain, which are defined as zero heat flux boundary condition.

The solution of the two-dimensional steady inverse heat transfer problem regarding this application comprehends transforming Eq. (1) in a linear form such as:

$$[R]\{S\} = \{\theta\} \quad (3)$$

This equation provides that, once the inverse of the thermal resistance matrix  $R$  is known and the normalized temperature profile is obtained (by measurements or any other technique), a vector containing the power map of a 2D heat source  $S$  can be easily obtained.

However, this problem is considered as an ill-posed problem according to Cochran *et al.* (2010), Nowroz (2014), Okamoto (2005), Qi

*et al.* (2010) and many others. Even if the problem physics ensures that there is at least one solution that satisfies this equation, the unity and stability criteria cannot be assured for most 2D inverse heat transfer problems (Okamoto, 2005, and Qi *et al.*, 2010). This becomes a major problem since most modeling and measurement techniques rely on approximations that result in slight differences obtained when using different methodologies. These small discrepancies, allied to high sensitivity, often result in inverse solutions that are significantly distant from the exact solution of the inverse problem.

So, to obtain better approaches to these solutions, they are usually obtained through a minimization least-squares problem defined such as:

$$\begin{aligned} \min \quad & \|[R]\{S\} - \{\theta\}\|_2^2 \\ \text{s.t.} \quad & \sum S_i = S_{total} \\ & S_i > 0 \end{aligned} \quad (4)$$

The goal of this minimization problem is to minimize the error between the estimated solution and the measured temperatures, restricting the solution using constraints, such that the sum of all source terms is equal to the total power emitted by the electronic device and that all source terms are necessarily non-negative.

So, the use of step-by-step solutions to these minimization problems considers directly the use of constraints in order to restrict the obtained solutions using previously known information of the physical problem, such as the inexistence of negative heat source terms, or the total thermal power emitted obtained through an energy balance. This use of constraints is regarded as beneficial, reducing the occurrence of ill-posed solutions (Nowroz, 2014, and Reda, 2011).

So, it is possible to obtain this solution using a step-by-step least-squares linear constrained solver, such as the MATLAB *lsqlin* function (Dev *et al.*, 2013). This approach neglects the use of regularization

\* Corresponding author. Email: rodrigovidonsky@gmail.com

techniques, relying only on conditioning techniques and on the constraints to obtain a stable solution process.

Other approaches (Cochran *et al.*, 2010, and Okamoto, 2005) uses a Tikhonov regularized form of the minimization problem, such as:

$$\begin{aligned} \min \quad & \left\| [R] \{S\} - \{\theta\} \right\|^2 + \alpha \|S\|_2^2 \\ \text{s.t.} \quad & \sum S_i = S_{total} \\ & S_i > 0 \end{aligned} \quad (5)$$

However, once the regularized objective function problem can be rewritten as a quadratic equation, other step-by-step algorithms, such as quadratic programming, also can be used to solve this problem.

The proposition of the present article consists in using a previously established heat source term to obtain an inverse solution using different solution methods. This problem is known as an inverse crime (Kaipio and Somersalo, 2004, and Siltanen, 2010). The use of these methods will result in a very small difference, but enough to disturb the solution process. The main goal of the present study is to present the effects obtained with the use of step-by-step algorithms incorporating often used constraints, with and without the introduction of regularization techniques, such as the Tikhonov regularization.

## 2. PROBLEM DESCRIPTION

To create a model that could describe accurately the dimensional issues associated with a two-dimensional heat transfer problem, such as a computer microprocessor, it was elaborated a flat surface containing positive heat source terms. The heat source characteristics, such as dimensions, magnitude, and spatial distribution, were based in both Hamann *et al.* (2006) and Reda (2011), since the dimensions of the model and the heat source magnitude are equivalent to the die of the IBM dual-core microprocessor PowerPC® 970 FX specifications (IBM Corp., 2006), while the heat source spatial distribution comprises two regions containing heat source terms with different spatial frequency. Fig. 1 shows a visual representation of this model.

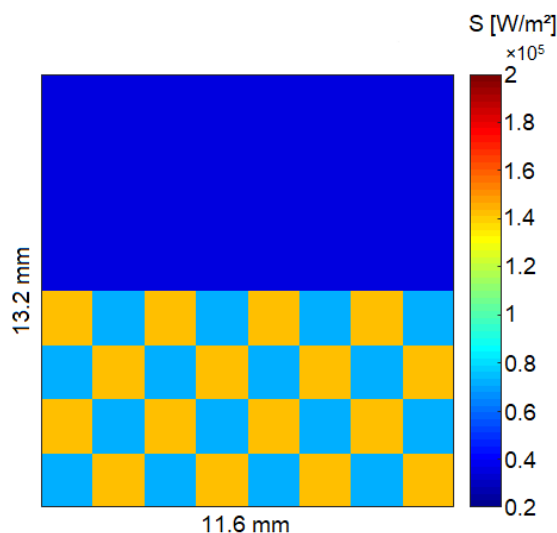


Fig. 1 Model representation

The sum of the net heat source values presented in Fig. 1 is 11 W, equal to the Thermal Design Power (TDP) of the PowerPC® 970 FX microprocessor (Stanford VLSI Group, 2019).

Also, to emulate the thermal diffusion due to heat conduction and the heat dissipation required for reaching steady-state condition, it is important to define a thermal conductivity to the material of the surface

and a dissipation term. For simplicity, it is assumed as homogeneous along the entire surface and equal to the thermal conductivity of the silicon, which is the base material used to fabricate microprocessors. So, it is defined that the thermal conductivity of the entire surface is constant and equal to 148 W/(m.K) (Plawsky, 2014).

For the dissipation term, in a real microprocessor, it would be necessary to represent the heat dissipation effect provided by the internal heat spreader (IHS) of the microprocessor, which, in most cases, is directly in contact with the die of the micro-processor. However, in situations involving direct die cooling, the microprocessor die could be able to dissipate heat directly to a fluid flow through convection heat transfer. This reduces the problem of defining the dissipation term to the definition of a convection heat transfer coefficient.

For liquid flow, usually the convection heat transfer coefficient obtained is in the range between 100 and 20000 (Incropera *et al.*, 2007). Also, according to the datasheet of the PowerPC® 970 FX (IBM Corp., 2006), the application temperature of this processor is 105°C and its storage temperature cannot exceed 125°C. So, the convection heat transfer coefficient is defined respecting this range, so that it results in a maximum temperature along the surface into the range between 105~125°C. The value of 1000 W/m²K was tested and satisfied both these conditions.

Once these conditions are defined, the solution of the direct problem was obtained using the finite differences method (FDM) using quadratic elements, such that the nodes were positioned at the center of each element. The boundary condition was defined as adiabatic by positioning ghost cells next to the border elements with equal temperature to the adjacent element, representing a null temperature gradient.

Also, from a grid independence analysis executed for 20x20, 40x40 and 60x60 elements grids, it is observed that the difference obtained when refining the grid from the 40x40 elements grid to the 60x60 elements grid is smaller than 1% of the temperature obtained, proving independence, so that the 40x40 elements grid could be defined as satisfactory. So, for a reference temperature of 20°C, the solution of the direct problem for a 40x40 elements grid using FDM can be seen in Fig. 2.

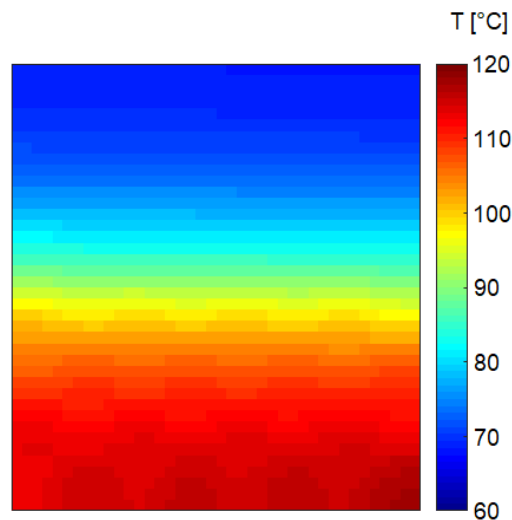


Fig. 2 Temperature distribution obtained using FDM

Once the model was correctly physically defined, it became necessary to obtain a temperature distribution containing a modeling error. This modeling error provides that the step-by-step solution of the inverse problem is not direct and will need to converge to the closest possible solution of the exact solution. This modeling error is obtained by solving the direct problem using CFD.

So, the commercial package ANSYS™ was selected for the creation of a CFD model. The software ICEM CFD® was used for the creation of a computational grid, while the software ANSYS CFX® was used for the application of the initial and boundary conditions and the solution of the conservation equations.

The same grid independence analysis is performed to grids having 20x20, 40x40, and 60x60 elements, obtaining that the 40x40 grid also is sufficiently refined to provide a solution within a 1% precision.

In the CFX, it is also important to define the solution controls for the numeric solution of the conservation equations of the problem to lead to a converged solution. For this, it is necessary to define four main configurations: Advection scheme, residual convergence control, maximum number of iterations, and numeric timescale.

The selection of the advection scheme consists in the choice of a blend factor  $\beta$  and a nodal gradient  $\nabla\phi$  for a variable  $\phi$  to be applied to the solution of the advection problem posed for a variable  $\phi$  such as:

$$\phi_{ip} = \phi_{up} + \beta \nabla\phi \cdot \Delta\vec{r} \quad (6)$$

Where  $\phi_{ip}$  is the value of the variable  $\phi$  at the integration point,  $\phi_{up}$  is the value of the variable  $\phi$  at the upwind node and  $\Delta r$  is the vector from the upwind node to the integration point.

The computational software ANSYS CFX® (ANSYS INC., 2009) provides three advection schemes for the solution of the CFD problem: Upwind ( $\beta = 0$ ), Specified Blend Factor ( $0 \leq \beta \leq 1$ ) and High-Resolution ( $\beta$  is computed through a nonlinear function at each node, such that  $\beta \rightarrow 1$  without introducing new extrema). The High-Resolution scheme was adopted in agreement with Choudhary *et. al.* (2021) and several other studies, providing the best option for reducing discretization errors.

The residual convergence control was set using the orders of magnitude of the problem such that the maximum RMS residual is defined as  $10^{-6}$ . Also, the maximum number of iterations was set as 1000, although the residual convergence control was reached in every simulation before those iterations reached their maximum. The numeric timescale was set as automatic.

So, also for a reference temperature of 20°C, the solution of the direct problem for a 40x40 elements grid using CFD can be observed in Fig. 3.

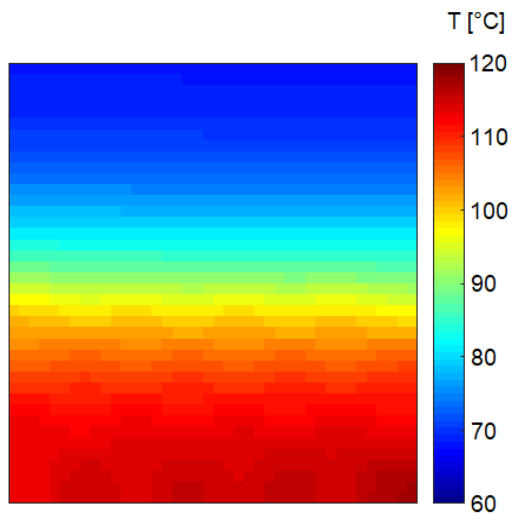


**Fig. 3** Temperature distribution obtained using CFD

The absolute modeling error obtained comparing the direct solution of the heat transfer problem using FDM or CFD can be observed in Fig. 4. The greater values of the modeling error are concentrated in the region

with the higher spatial frequency of different heat source terms. However, the order of magnitude of the obtained errors is between 0.1% and 0.2% of the temperature for the entire surface.

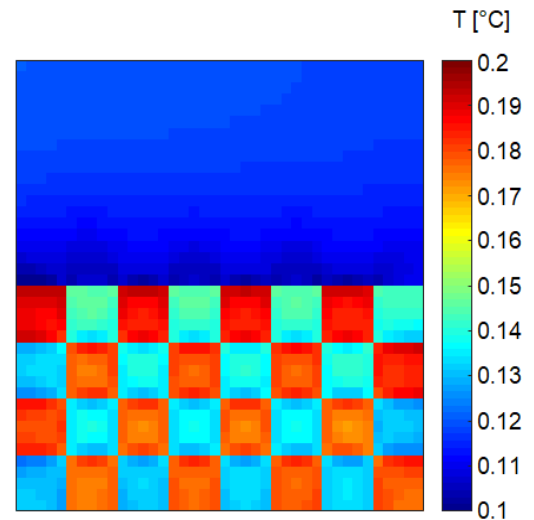


**Fig. 4** Absolute modeling error

Once there are two distinct temperature distributions obtained through different methods, four different approaches are defined to obtain the solution for the inverse heat transfer problem from the temperature distribution obtained from the CFD solution.

The first approach consists in using the direct inverse of the thermal resistances matrix  $R$  to obtain the heat sources distribution  $S$ . This can be done by directly multiplying a matrix  $A$  obtained from the FDM discretization with the vectorized and normalized temperature distribution  $\theta$  obtained from the CFD solution, such that:

$$\{S\} = [A]\{\theta\} \quad (7)$$

$$[R]^{-1} = [A] \quad (8)$$

Since this solution is obtained without using any inversion technique, it corresponds to the best solution obtainable by any algorithm using these input parameters. Also, this method is direct, dismissing any kind of restriction.

The second approach consists in solving the minimization least-squares problem as defined in Eq. (4) using a step-by-step linear optimization algorithm, such that the solution of this minimization problem consists in an approach of the best solution of the heat sources distribution  $S$  with a minimized error. This solution is obtained using the MATLAB lsqin function.

According to Mathworks Inc. (2019) the lsqin function consists of a linear least-squares solver with bound and linear constraints. It is suitable for least-squares curve fitting problems of the form:

$$\begin{aligned} \min \quad & \frac{1}{2} \|[C]\{x\} - \{d\}\|_2^2 \\ \text{s.t.} \quad & [F]\{x\} \leq \{g\} \\ & [F_{eq}]\{x\} = \{g_{eq}\} \\ & \{lb\} \leq \{x\} \leq \{ub\} \end{aligned} \quad (9)$$

The use of constraints allows the problem to introduce a priori known information to restrict the number of possible solutions, and, theoretically, improving the solution process.

Usually, the adopted constraints restrict the heat sources distribution  $S$  to a matrix with only non-negative values, in the form of a boundary constraint, such that:

$$\{S\} \geq 0 \quad (10)$$

And restrict the sum of all heat sources distribution  $S$  terms as equal to the total power consumption of the entire surface, such that:

$$\{1 \cdots 1\} \{S\} = S_{total} \quad (11)$$

Such constraints are also used in Cochran *et al.* (2010) and Reda (2011).

This method uses an interior-point-convex algorithm, which enables the use of the aforementioned constraints. This algorithm is defined such that the minimization linear least-squares problem defined in Eq. (9) is converted to the quadratic form:

$$\min_x \frac{1}{2} \{x^T\} [H] \{x\} + \{f^T\} \{x\} \quad (12)$$

$$[H] = 2[C]^T [C] \quad (13)$$

$$\{f\} = -2[C]^T \{d\} \quad (14)$$

Next, the third approach consists in solving the regularized form of the inverse problem as defined in Eq. (5) directly. The application of regularization techniques looks to improve the solution process of an ill-posed inverse heat transfer problem by a similar better-posed problem with the same solution as the original problem.

The Tikhonov regularized form of the minimization least-squares problem as defined in Eq. (5) is known for providing a direct solution using an SVD decomposition of the thermal resistance matrix  $R$ , such as:

$$\{S_\alpha\} = [V] \text{diag} \left[ \left( \frac{d_i^2}{d_i^2 + \alpha} \right) \left( \frac{1}{d_i^2} \right) \right] [U]^T \{\theta\} \quad (15)$$

This solution also dismisses the use of constraints.

Finally, the fourth approach consists in solving the regularized form of the inverse problem as defined in Eq. (5) using a quadratic step-by-step algorithm. The regularized form of the optimization problem can be rewritten to assume the same form presented in Eq. (12). However, it incorporates the regularization parameter in the Hessian matrix  $H$  resulting in the form:

$$[H] = 2[C]^T [C] + \alpha [I] \quad (16)$$

Such that  $I$  is an identity matrix with the size of  $C$ . This objective function remains a quadratic function that can be solved using quadratic programming algorithms, such as the MATLAB® *quadprog* function.

Furthermore, since the aforementioned interior-point-convex algorithm can deal with quadratic minimization problems, this algorithm is also used to solve the regularized minimization problem through quadratic programming. The same constraints that can be evaluated with the linear least-squares solver can also be evaluated with this algorithm.

### 3. RESULTS

The use of the first approach in order to solve the inverse heat transfer problem enables that two important variables are verified: the thermal resistance matrix  $R$  and the heat sources distribution  $S$  corresponding to the best obtainable solution using the thermal resistance matrix obtained from the FDM discretization.

In order to verify the validity of the thermal resistance matrix, we initially used the solution obtained through the FDM as an input parameter for the solution of the inverse heat transfer problem using the first approach.

The obtained heat sources distribution using this approach is significantly close to the heat sources distribution presented in Fig. 1, such that a qualitative image of both sources is practically identical. So, Fig. 5 presents the corresponding heat source difference distribution  $\Delta S$  between the two distributions. It can be observed that the maximum difference between the two distributions is close to three orders of magnitude smaller than the minimum values of the actual heat sources distribution so that it can be assured that the thermal resistance matrix can accurately represent the thermal diffusion and the convection dissipation phenomena along the surface.

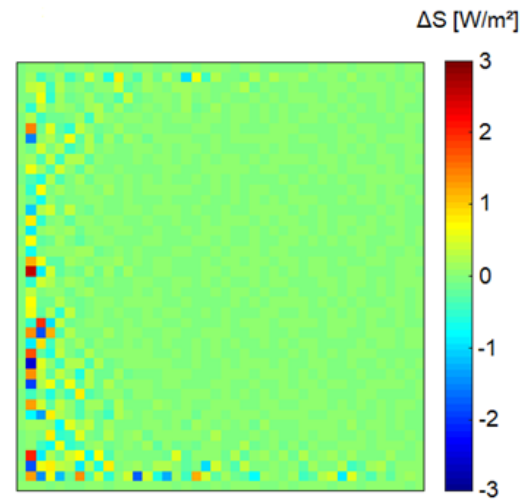


**Fig. 5** Heat sources difference distribution: actual heat source distribution and first approach FDM

Next, once this thermal resistance matrix is verified, a direct solution for the inverse problem can be obtained for the temperature distribution resulting from the CFD direct solution. Since Fig. 4 presents that there is a slight difference between the obtained temperature distributions for the two different modeling techniques, it is expected that the heat sources distribution obtained through this approach is different from the actual heat sources distribution.

Figure 6a presents the heat sources distribution obtained through the first approach using the temperature distribution resulting from the CFD direct solution. As expected, there is a significant difference between the actual heat sources distribution and the obtained heat distribution, with heat source terms near the borders with values two orders of magnitude greater than the heat source terms present in the actual heat sources distribution of Fig. 1.

However, Fig. 6b presents the same temperature distribution using the same scale used for the actual heat sources distribution presented in Fig. 1 (between  $2 \times 10^5$  and  $2 \times 10^6$ ), revealing that, far from the border region, the solution of the inverse problem using this approach succeeds in representing quite accurately the heat sources distribution. This distribution, however, seems to be subject to a low-pass filter effect. The mean relative error in this region is  $\pm 3.95\%$ .

Also, Fig. 6c presents a distribution revealing only the location of the positive and negative terms for this solution. From this figure, it can be observed that some of the ghost cells used for the application of the adiabatic boundary conditions assumed negative values to compensate for the high sensitivity obtained through the inversion of the modeling error.

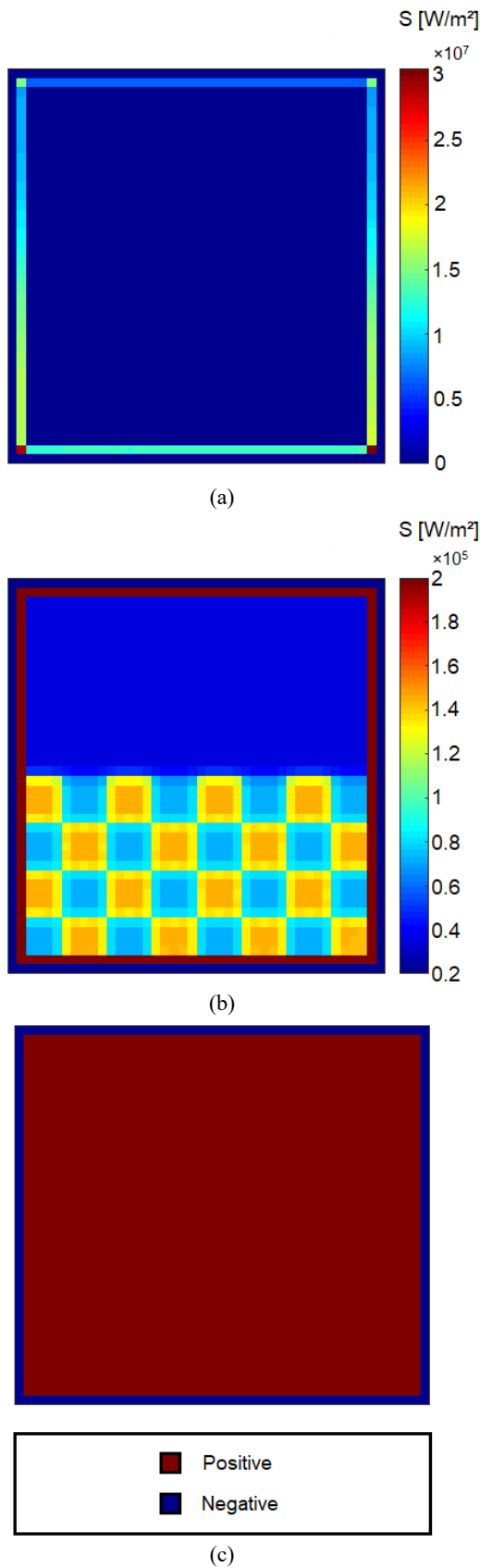
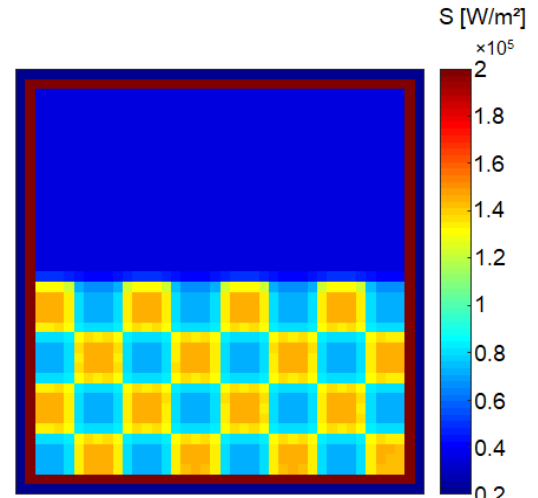


**Fig. 6** First approach heat sources distribution

Next, the second approach is applied to obtain the heat sources distribution using a step-by-step linear optimization algorithm. The

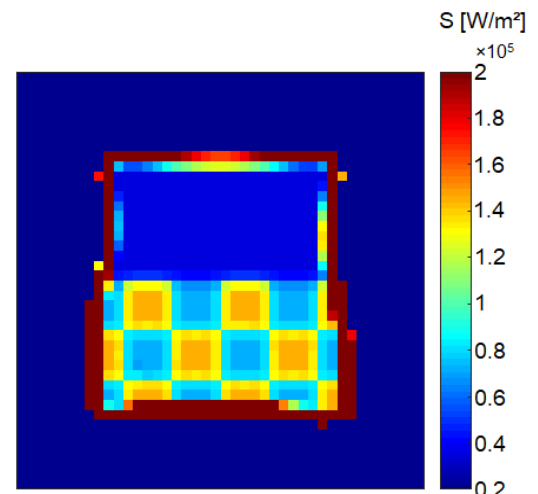
maximum number of iterations and the function tolerance remained at the automatic values (200 and  $2.22 \times 10^{-14}$ ) since all solution processes succeeded to converge to their corresponding minima within these stopping conditions.

Figure 7 presents the heat sources distribution obtained through the unrestricted solution in the actual heat sources distribution scale (between  $2 \times 10^5$  and  $2 \times 10^6$ ). It can be observed from a comparison between Figs. 6 and 7 that the unrestricted step-by-step algorithm obtains a solution that is very close to the solution obtained through the first approach.



**Fig. 7** Unrestricted second approach heat sources distribution

The introduction of the constraints from Eqs. (10) and (11) (therefore named constraints CI and CII) to the second approach can be observed in Figs. 8 to 12. Fig. 8 correspond to the heat sources distribution incorporating only the CI non-negative restriction. Fig. 9 correspond to the heat sources distribution incorporating only the CII sum of all heat sources restriction, adopting the heat source sum from the actual heat sources distribution presented in Fig. 1 (therefore named as CII-A). Fig. 10 correspond to the heat sources distribution incorporating only the CII sum of all heat sources restriction and adopting the heat source sum from the inverse heat transfer problem solution presented in Fig. 6 (therefore named as CII-B). Figs. 11 and 12 adopt both the CII non-negative restriction and the CII sum of heat sources restriction, using the CII-A sum of all heat sources (Fig. 12) or the CII-B sum of all heat sources (Fig. 13).



**Fig. 8** Restricted second approach heat sources distribution – constraint CI

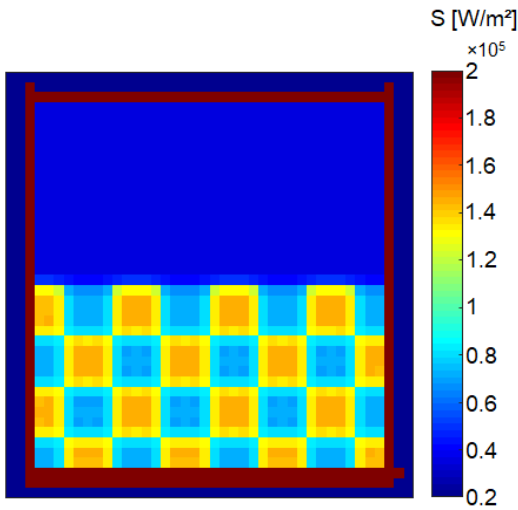


**Fig. 9** Restricted second approach heat sources distribution – constraint CII-A

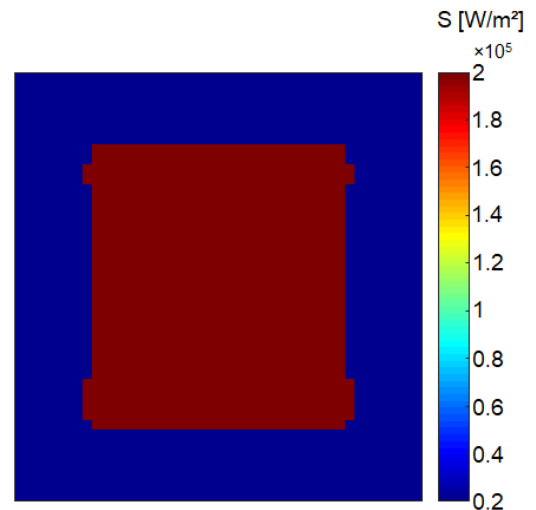


**Fig. 12** Restricted second approach heat sources distribution – constraints CI and CII-B

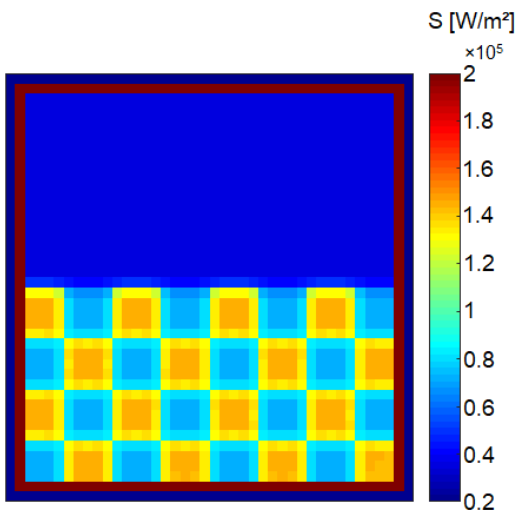


**Fig. 10** Restricted second approach heat sources distribution – constraint CII-B

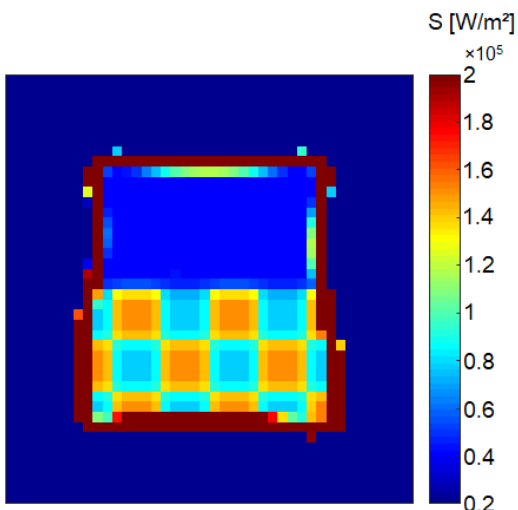


**Fig. 11** Restricted second approach heat sources distribution – constraints CI and CII-A

From Figs. 8 to 12, it can be observed that none of these constraints could significantly upgrade the solution obtained through the solution of the unrestricted inverse problem both by the direct solution or by the unrestricted step-by-step linear least-squares solution presented in Figs. 6 and 7. Also, Fig. 12 present that the use of the CI non-negative restriction and the CII-B sum of heat sources restriction completely ruins the solution.

In all studied cases in which the CI non-negative terms restriction was used, the obtained solution corresponding to a limited solution of the inverse heat transfer problem, confined to the central area of the problem, while the remaining terms around the border region were fixed as zero. This is a direct consequence of the absence of the small negative terms adopted in the ghost cells used in the FDM direct solution. These terms compensated part of the modeling error of the problem by exploiting the high sensitivity of this problem to counterbalance the effect of the high heat source terms found near the borders of the problem. When these terms are set to be non-negative, the optimization algorithm could not find better solutions for the border regions than setting them all as zero, due to the modeling error, so the algorithm could not compensate for the high sensitivity resulting from the modeling error and provided this limited solution.

On the other hand, the adoption of the CII sum of heat sources restriction had different effects. Fig. 9 shows that the heat sources distribution obtained using the actual heat sources distribution adopted for this study as the CII sum of all heat sources restriction resulted in a different solution. This solution preserves a considerable area of the best solution obtained through the unrestricted problem and the heat source terms in the ghost cells are closer to zero than the unrestricted solution. This effect can be observed in Fig. 13a (unrestricted problem) and 13b (restricted problem – CII-A sum of all heat sources restriction).

Still, it can be observed the creation of an additional layer of terms in the border region containing a disturbed solution with negative heat source terms. This is a direct consequence of this restriction, which tries to compensate the smaller sum of all heat sources with negative terms in the heat sources distribution.

Also, from Fig. 10, it can be observed that the adoption of the CII-B restriction resulted in the same heat sources distribution obtained through the unrestricted problem.

The next step is the solution of the inverse problem using the third approach. This approach requires the estimation of the regularization parameter  $\alpha$ , which is performed by using the method *a posteriori* known as the Morozov discrepancy principle (Kaipio and Somersalo, 2004). This principle defines that the regularization parameter must be defined

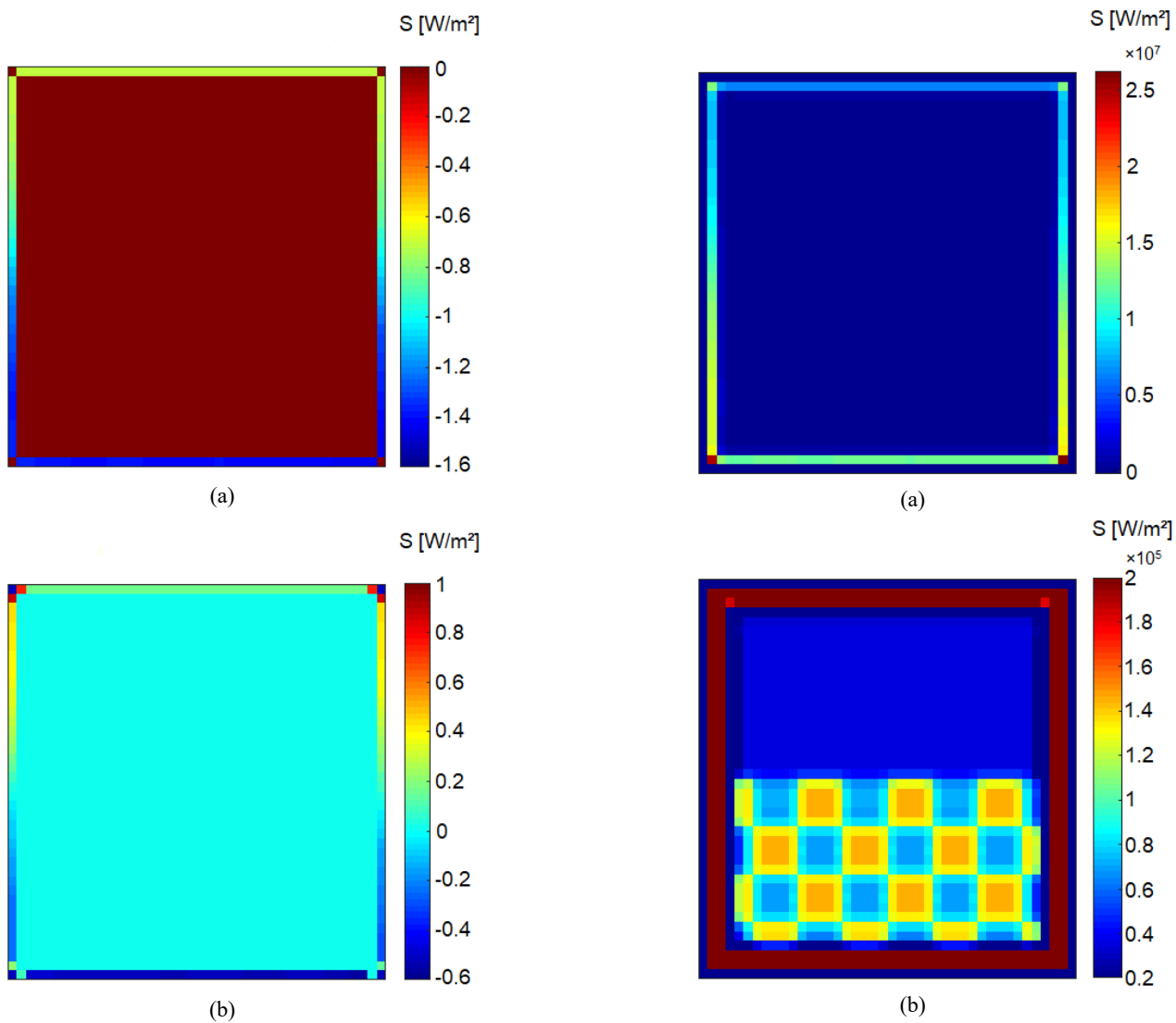


**Fig. 13** Ghost cells heat source terms

defined such that the L2 norm of the errors due to measurements or numeric methods is equal to the regularization parameter. So:

$$\alpha = \left\| [R] \{S(e)\} - \{\theta\} \right\|_2 \quad (17)$$

The numeric implementation of this principle is described in Siltanen (2010) and corresponds to the location of the zero of a function of the regularization parameter  $\alpha$ . This is performed using the absolute modeling error distribution presented in Fig. 4. The resulting regularization parameter obtained is  $1.2026 \times 10^{-16}$ .

Then, the solution of the inverse heat transfer problem is reduced to the application of Eq. (15). The resulting heat sources distribution can be observed in Fig. 14a. The effect obtained through the introduction of the regularization is similar to the effect obtained using an additional low-pass filter. The modeling error is not eliminated by the regularization process, once it is recognized as part of the original problem, due to the nature of the error. Instead, the regularization tends to smooth the gradients along the heat sources distribution, isolating the central areas of the heat sources distribution with a layer of negative heat source terms, as presented in Figs. 14b and 14c. Also, in the ghost cells, the heat source terms remained all negative.

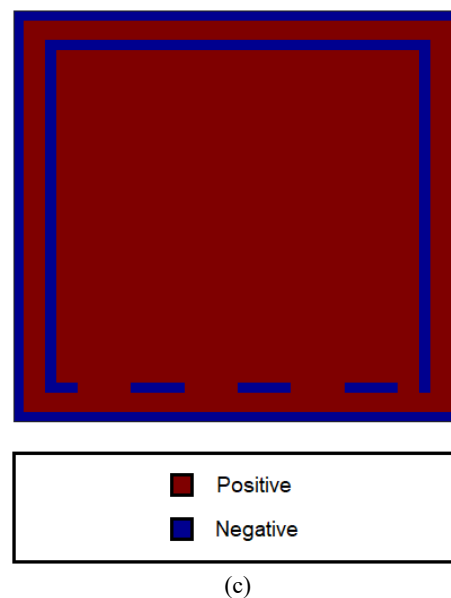


**Fig. 14** Third approach heat sources distribution

Finally, the fourth approach is applied to solve the regularized inverse heat transfer problem using quadratic programming, resulting in the heat sources distributions presented in Fig. 15 for the unrestricted solution and in Figs. 16 to 20 for the same constraints adopted for the second approach. The maximum number of iterations, the function tolerance, and the constraint tolerance remained at the automatic values ( $200$ ,  $1 \times 10^{-8}$ , and  $1 \times 10^{-8}$ ) since all solution processes succeeded to converge to their corresponding minima within these stopping conditions.

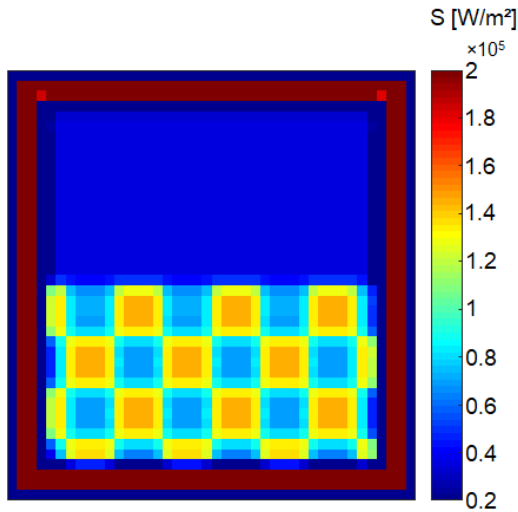


**Fig. 15** Unrestricted fourth approach heat sources distribution

It must be noticed that the same effects observed when comparing the results of the first and the second approach repeated them when comparing the results of the third and the fourth approach regarding the use of constraints. Once again, it can be observed that:

- none of these constraints could significantly upgrade the solution obtained through the solution of the unrestricted inverse problem both by the direct solution or by the unrestricted step-by-step quadratic programming solution;
- the use of the CI non-negative restriction and the CII-B sum of heat sources restriction completely ruins the solution;
- for all studied cases in which the CI non-negative terms restriction was used, the obtained solution corresponding to a limited solution of the inverse heat transfer problem, confined to the central area of the problem, while the remaining terms around the border region were fixed as zero;
- using only the CII-A restriction, the solution of the inverse heat transfer problem of Fig. 17 resulted in a heat sources distribution presenting a considerable area of the best solution obtained through the unrestricted problem preserved and the heat source terms in the ghost cells closer to zero than the unrestricted solution. This solution also presents an additional layer of terms in the border region containing a disturbed solution with negative heat source terms;
- the adoption of the CII-B restriction resulted in the same heat sources distribution obtained through the unrestricted problem.

#### 4. CONCLUSIONS

The present study succeeded in obtaining two different temperature distributions to simulate a modeling error for the direct solution of a heat transfer problem. The solution of the corresponding inverse heat transfer problem of these temperature distributions revealed this modeling error from CFD to FDM solution, which consists in obtaining a low-pass filtered version of the actual heat sources distribution with a disturbed border region. This modeling error allowed that the study of the use of

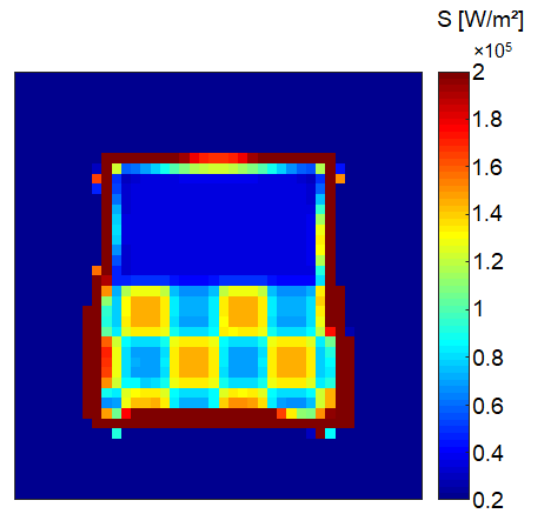


**Fig. 16** Restricted fourth approach heat sources distribution – constraint CI

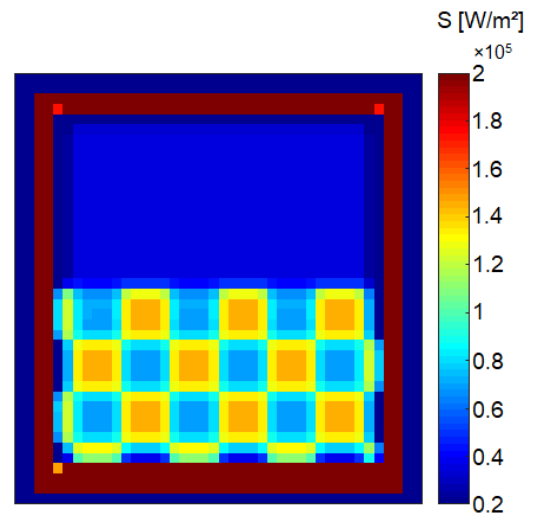


**Fig. 17** Restricted fourth approach heat sources distribution – constraint CII-A

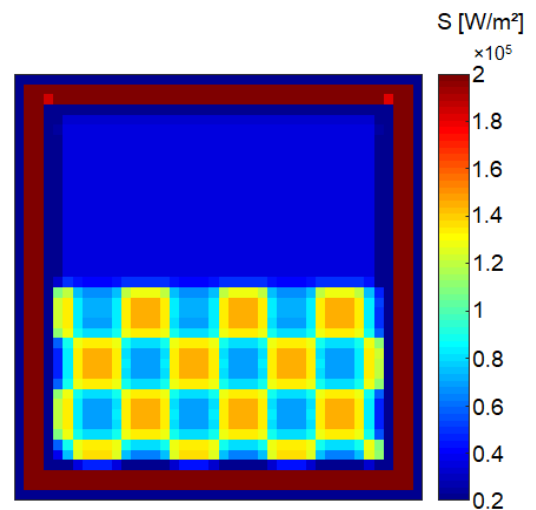


**Fig. 18** Restricted second approach heat sources distribution – constraint CI

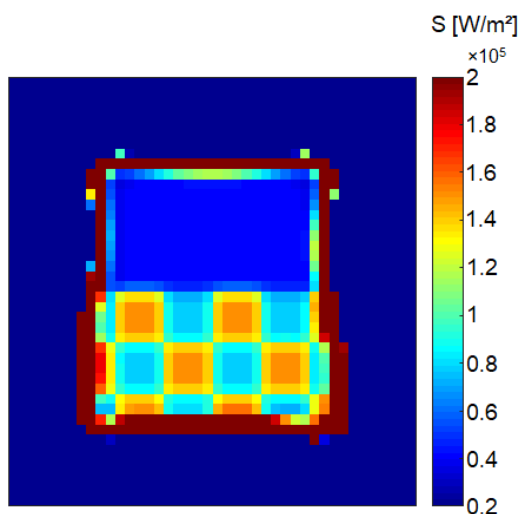


**Fig. 19** Restricted fourth approach heat sources distribution – constraints CI and CII-A

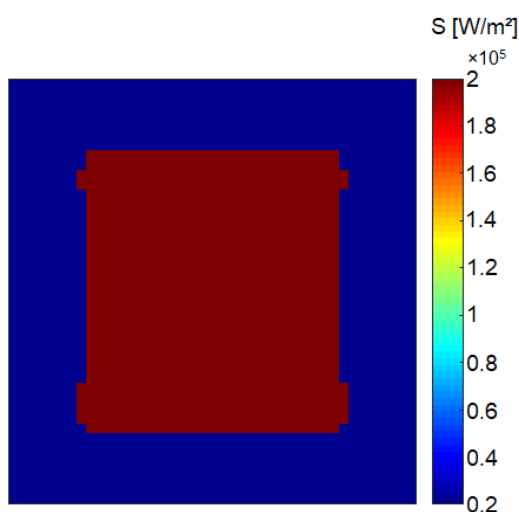


**Fig. 20** Restricted fourth approach heat sources distribution – constraints CI and CII-B

constraints for the solution of the inverse heat transfer problem was compared to unrestricted solutions.

It must be noticed that the solution of the inverse heat transfer problem obtained through unrestricted step-by-step algorithms is numerically identical to the direct solution of this problem. Also, both provided a reasonable and manageable solution for the inverse heat transfer problem, even in the presence of this modeling error.

This use of constraints, which is usually regarded as beneficial and able to reduce the occurrence of ill-posed solutions led the step-by-step algorithm to worse solutions than the unrestricted algorithm in the presence of this modeling error. The high sensitivity of the problem led to the adoption of negative heat source terms along the ghost cells used for the application of the boundary conditions, helping to compensate for the disturbance produced in the border region by this error. The use of constraints denies the adoption of these negative terms, so the algorithm defined all the border section of the heat sources as zero in order to obtain a valid solution, obtaining so a reasonable solution confined to the central area of the problem.

So, it was concluded that the CI non-negative terms restriction is harmful to the solution of the inverse heat transfer problem containing a modeling error, once it neglects that, in order to compensate the high

sensitivity of this problem, the solution process may place negative terms in support cells to reach better solutions.

Also, the CII sum of heat sources restriction is less harmful to the solution of the inverse heat transfer problem containing a modeling error than the CI non-negative terms restriction, once it permits that negative heat source terms still compensate the modeling errors. However, the smaller this sum is defined, the farther from the direct solution of the heat transfer problem the resulting solution becomes.

Finally, future studies should address the use of different regularization techniques and different constraints to suppress the modeling error and obtain a closer solution to the actual heat sources distribution. The use of the CII-A restriction seems to provide a better perspective than the CI for this further development.

## ACKNOWLEDGEMENTS

Authors would like to acknowledge Coordenação de Aperfeiçoamento de Pessoal de Nível Superior (CAPES) for supporting the research.

## NOMENCLATURE

$A$	thermal diffusion matrix (W/K)
$k$	thermal conductivity (W/m·K)
$f$	quadratic first-order coefficient
$F$	linear first-order coefficient
$g$	linear zero-order coefficient
$h$	convective heat transfer coefficient (W/m <sup>2</sup> ·K)
$H$	hessian matrix
$lb$	optimization lower boundary
$R$	thermal resistance matrix (K/W)
$S$	heat sources distribution (W)
$T$	temperature (K)
$U$	singular values decomposition matrix
$ub$	optimization upper boundary
$V$	singular values decomposition matrix
$x$	optimization variable

### Greek Symbols

$\alpha$	regularization parameter
$\beta$	blend factor
$\theta$	normalized temperature (K)

### Subscripts

$d$	singular matrix diagonal values
$e$	electron
$l$	lattice
$\infty$	ambient environment

## REFERENCES

- Ansys Inc., 2013, “ANSYS CFX-solver theory guide”. ANSYS CFX Release, v. 15.0, p. 338–340
- Cochran, R.; Nowroz, A. N.; Reda, S., 2010, “Post-silicon power characterization using thermal infrared emissions”. *Low-Power Electronics and Design (ISLPED), 2010 ACM/IEEE International Symposium*, 331–336.  
<https://doi.org/10.1145/1840845.1840914>
- Choudhary, K.D., Shyam, S.S., Dasgupta, M.S., 2022, “A comparison of the equilibrium and the droplets based non-equilibrium compressible phase change solvers for condensation of carbon dioxide inside nozzles”. *Frontiers in Heat and Mass Transfer*, **16**(14), 1-10.  
<http://dx.doi.org/10.5098/hmt.16.14>
- Dev, K.; Nowroz, A. N.; Reda, S., 2013, “Power mapping and modeling of multi-core processors”. *Proceedings of the International Symposium on Low Power Electronics and Design*, 39–44.  
<https://doi.org/10.1109/ISLPED.2013.6629264>

Gulia, V., Sur, A., 2022, "A comprehensive review on microchannel heat exchangers, heat sink, and polymer heat exchangers: Current state of the art". *Frontiers in Heat and Mass Transfer*, **18**(40), 1-10.  
<http://dx.doi.org/10.5098/hmt.18.40>

Hamann, H. F. *et al.*, 2006, "Spatially-resolved imaging of microprocessor power (SIMP): Hotspots in microprocessors". *Thermomechanical Phenomena in Electronic Systems -Proceedings of the Intersociety Conference*, **2006**, 121–125.  
<https://doi.org/10.1109/ITHERM.2006.1645331>

IBM Corporation, 2006, "IBM PowerPC® 970FX RISC Microprocessor Data Sheet". 1–74.

Incropera, F.P., DeWitt, D.P., Bergman, T.L., and Lavine, A.S., 2011, *Fundamentals of Heat and Mass Transfer*, 7<sup>th</sup> ed., John Wiley & Sons, Hoboken, NJ.

Kaipio, J., Somersalo, E., 2004, "Statistical and computational inverse problems". *Applied Mathematical Sciences*, **160**, Springer, 2004.

Mathworks Inc., 2019, "Optimization Toolbox Documentation".

Nowroz, A. N., 2014, "Power Mapping of Computing Devices: Fundamentals and Applications". Providence: Brown University, 2014, 198 p., Ph.D Thesis – School of Engineering, Brown University, Providence, Rhode Island.

Okamoto, K., 2005, "Optimal numerical methods for inverse heat conduction and inverse design solidification problems". Pullmann: Washington State University, 2005, 167 p., Ph.D Thesis – School of Mechanical and Materials Engineering, Washington State University, Pullmann, Washington.

Plawsky, J. L., 2014, *Transport phenomena fundamentals*. 3<sup>rd</sup> ed., CRC Press.

Qi, Z.; Meyer, B. H.; Huang, W.; Ribando, R. J.; Skadron, K.; Stan, M. R., 2010, "Temperature-to-power mapping". *Proceedings - IEEE International Conference on Computer Design: VLSI in Computers and Processors*, 384–389.  
<https://doi.org/10.1109/ICCD.2010.5647690>

Reda, S., 2011, "Thermal and power characterization of real computing devices". *IEEE Journal on Emerging and Selected Topics in Circuits and Systems*, **1**(2), 76–87.  
<https://doi.org/10.1109/JETCAS.2011.2158275>

Siltanen, S., 2010, "Computational Inverse Problems". *Lecture Notes*, **14**.  
<https://wiki.helsinki.fi/download/attachments/63749375/IPnotes14.pdf> (accessed January 31, 2019).

Stanford VLSI Group, 2019, "CPU DB - Looking At 40 Years of Processor Improvements | A complete database of processors for researchers and hobbyists alike".  
<http://cpudb.stanford.edu/processors/306> (accessed January 31, 2019).

Velardo, J. *et al.*, 2021, "Thin thermal management modules using flattened heat pipes and piezoelectric fans for electronic devices". *Frontiers in Heat and Mass Transfer*, **17**(1), 1-11.  
<http://dx.doi.org/10.5098/hmt.17.1>